Applied Catalysis B: Environmental 158–159 (2014) 301–307

Contents lists available at ScienceDirect

Applied Catalysis B: Environmental

journal homepage: www.elsevier.com/locate/apcatb

Visible-light-driven photocatalytic inactivation of *E. coli* by Ag/AgX-CNTs (X = Cl, Br, I) plasmonic photocatalysts: Bacterial performance and deactivation mechanism

Huixian Shi [a], Guiying Li [a], Hongwei Sun [a,d], Taicheng An [a,*], Huijun Zhao [b], Po-Keung Wong [c,**]

[a] State Key Laboratory of Organic Geochemistry, Guangzhou Institute of Geochemistry, Chinese Academy of Sciences, Guangzhou 510640, China
[b] Centre for Clean Environment and Energy, Griffith Scholl of Environment, Griffith University, Queensland 4222, Australia
[c] School of Life Sciences, The Chinese University of Hong Kong, Shatin, NT, Hong Kong SAR, China
[d] University of Chinese Academy of Sciences, Beijing 100049, China

ARTICLE INFO

Article history:
Received 21 February 2014
Received in revised form 18 April 2014
Accepted 20 April 2014
Available online 26 April 2014

Keywords:
Silver halides
Photocatalytic activity
Mechanism
Bacterial inactivation
Visible light

ABSTRACT

In this work, an effective photocatalytic inactivation of *Escherichia coli* K-12 was investigated using a series of synthesized Ag/AgX-CNTs (X = Cl, Br, I) composites as photocatalysts under visible light (VL) ($\lambda \geq 400$ nm) irradiation. The results showed that the visible-light-driven (VLD) Ag/AgBr-CNTs could completely photocatalytically inactivate 1.5×10^7 cfu mL^{-1} of *E. coli* within 40 min, which was superior to Ag/AgCl-CNTs and Ag/AgI-CNTs. Moreover, photocatalytic bactericidal mechanism of the Ag/AgX-CNTs was investigated by using various scavengers to remove the respective reactive species and at different wavelengths of VL. It was found that photocatalytic inactivation of *E. coli* was much more efficient under VL with 435 nm wavelength and the photogenerated holes played an important role in this photocatalytic inactivation system. In addition, the stability and deactivation mechanism of Ag/AgX-CNTs photocatalysts during photocatalytic bacterial inactivation were also studied, and the results showed that the organic debris of decomposed bacteria may be absorbed on the active sites of the photocatalysts leading to the decrease of the photocatalytic activity.

© 2014 Elsevier B.V. All rights reserved.

1. Introduction

With urbanization and industrialization, the environmental pollution caused by hazardous wastes has been become an overwhelming problem around the world [1]. Water is a basic commodity needed in ever-increasing quantities by human society. However, many water sources are polluted not only by various hazardous chemicals but also by pathogenic microorganisms [2,3]. Traditional water disinfection methods such as chlorination and ozonation have shown disadvantages related to the production of potentially hazardous disinfection byproducts [4,5]. Therefore, the development of more effective water purification technologies with or without hazardous disinfection byproducts has become an urgent issue. The semiconductor photocatalysis technique provides an environmentally friendly method for completely eliminating various contaminants. In 1985, Matsunaga et al. first reported that illuminated TiO_2 photocatalyst could kill bacterial cells in water [6]. Since then, photocatalysis was extensively studied and proved to be a cost-effective, safe and promising alternative for wastewater treatment and water purification, and numerous studies related to the bactericidal activity of TiO_2-based photocatalysts have been reported [7–10]. However, TiO_2 photocatalyst can only be activated in the UV-region, which is only about 4% of the solar spectrum. Therefore, the development of new and more efficient visible-light-driven (VLD) photocatalysts has become an attractive topic from the viewpoint of using solar energy [11].

Some researches showed that noble metal nanoparticles, such as Ag, Au and Pt, exhibited strong UV–vis absorption due to their plasmon resonance, which is produced by the collective oscillations of surface electrons [12–16]. Therefore, recently much more effort has been devoted to design Ag/AgX (X = Cl, Br, I) composite materials due to the surface plasmon resonance (SPR) of metallic Ag [1,17–20], which can dramatically enhance the absorption of visible light (VL) and provide new opportunities to develop VLD photocatalysts [21]. For example, it has been demonstrated

* Corresponding author. Tel.: +86 20 85291501; fax: +86 20 85290706.
** Corresponding author. Tel.: +852 3943 6383; fax: +852 2603 5767.
E-mail addresses: antc99@gig.ac.cn (T. An), pkwong@cuhk.edu.hk (P.-K. Wong).

http://dx.doi.org/10.1016/j.apcatb.2014.04.033
0926-3373/© 2014 Elsevier B.V. All rights reserved.

that Ag/AgX (X = Cl,Br) [14], Ag/AgBr/TiO_2 [19,22], and graphene sheets grafted Ag@AgCl [23] showed an enhanced VLD photocatalytic activity to degrade various organic pollutants in water. Also, Zhang et al. reported an effective photocatalytic bacterial inactivation using a AgBr-Ag-Bi_2WO_6 nanojunction system under VL irradiation (completely killed 5×10^7 cfu mL^{-1} *Escherichia coli* K-12 within 15 min) [24]. Hu et al. prepared a novel photocatalyst Ag/AgBr/TiO_2, which showed high inactivation efficiency for *E. coli* under VL irradiation [19]. However, to the best of our knowledge, the synthesis plasmon-induced VLD photocatalytic nanocomposites Ag/AgX-CNTs for photocatalytic inactivation of biohazards has not been reported yet.

On the other hand, photoinduced charge transfer behavior limits the promotion in the photoconversion efficiency and the reusability of Ag/AgX is not very well [19,24]. Therefore, loading Ag/AgX onto a suitable supporting material may provide an ideal solution to overcome above-mentioned drawbacks existed for this type photocatalysts. For instance, compared with bare Ag/AgX (X = Cl, Br), the fabricated plasmon-induced Ag/AgX loaded graphene oxide has significantly enhanced photocatalytic activity and stability [14]. CNTs has been frequently selected as a catalyst carrier owing to its hollow and layered structure as well as unique physical-chemistry properties [25,26]. In addition, CNTs can be believed to serve as electron acceptor to inhibit the recombination of photogenerated charges [27–29]. However, CNTs based photocatalysts by loading Ag/AgX onto CNTs has not yet been attempted to the water disinfection.

In the present paper, from kinetic and mechanistic viewpoints, the photocatalysts Ag/AgX-CNTs were employed to investigate photocatalytic inactivation performance using ubiquitous waterborne microorganism *E. coli* as a model bacterium under VL irradiation for the first time. The plasmon-induced photocatalytic inactivation mechanism of the bacteria by the prepared Ag/AgX-CNTs under VL irradiation was also proposed based on the scanning electron microscopic (SEM) analysis on the damage to the bacterial cell in conjugation with other experimental evidences, such as the role of reaction species (RSs), K^+ leakage and other information for example Fluorescence microscopic images and FT-IR spectra. Moreover, the stability of Ag/AgX-CNTs to inactivate bacteria cells in water was evaluated under VL irradiation, and the deactivation mechanism of photocatalysts was also discussed in detail.

2. Experimental

2.1. Preparation and characterization of photocatalysts

All of the reagents were analytical grade and used without further purification. The CNTs were pretreated by refluxing in the mixture of concentrated H_2SO_4 acid (95–98%) and HNO_3 (65–68%), and the Ag/AgX-CNTs photocatalysts were prepared by an ultrasonic assistant deposition-precipitation method according to our previous study [30]. The crystal phase composition, surface chemistry properties as well as surface structure of the photocatalysts before and after used were characterized by X-ray diffraction (XRD, Rigaku Dmax 2200 V X-ray diffractometer), X-ray photoelectron spectroscopy (XPS, S-520/INCA 300 spectrometer using 300 W Mg-Kα radiation, and the binding energies were referenced to the C1s line at 284.8 eV from adventitious carbon) and the Fourier transform infrared spectroscopy (FTIR, Bruker EQUINOX55 spectrometer). Photoluminescence (PL) spectra of the samples were obtained using a combined fluorescence lifetime and steady state spectrometer (FLSP920, Edinburgh instruments lid) under 290 nm emissions at 293 K, and the slit widths at the excitation and the emission of the spectrofluorimeter were 5.0 and 2.7 nm, respectively.

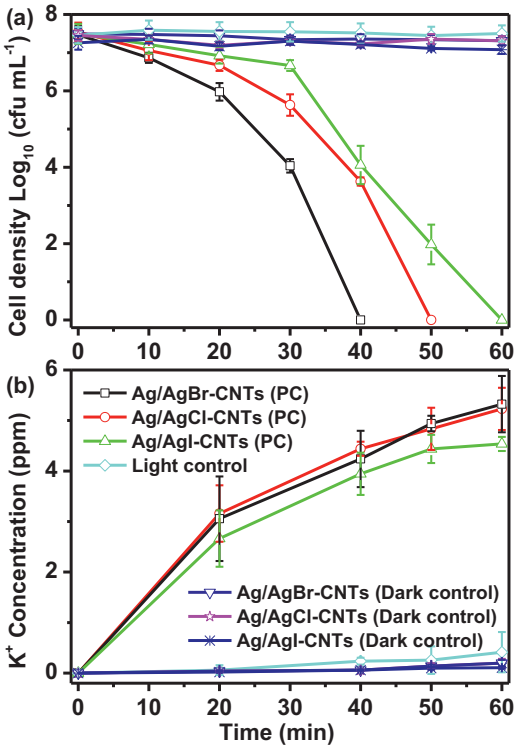

Fig. 1. Photocatalytic inactivation efficiency of *E. coli* by Ag/AgX-CNTs (X = Cl, Br, I) under visible light irradiation (a); potassium ion (K^+) leakage from *E. coli* under different conditions (b).

2.2. Photocatalytic disinfection performance

E. coli K-12 was chosen as a model bacterium to evaluate photocatalytic disinfection activity of the prepared photocatalysts. The light source (Fig. S1) was a 300 W Xenon lamp (PLS-SXE-300, Beijing Perfect Light Co. Ltd., Beijing) equipped with a UV cutoff filter ($\lambda < 400$ nm). The light intensity was kept about 60 mW cm^{-2}. The Xenon lamp with different cutoff filters (420, 450, 500, 435, 475, 520 and 550 nm, Beijing Perfect Light Co. Ltd., Beijing) was employed to study the effect of wavelength on photocatalytic inactivation of bacteria. The schematic diagram of the experimental setup was shown in Fig. S2. The detail procedure of photocatalytic inactivation was shown in Supporting Information.

3. Results and discussion

3.1. Photocatalytic disinfection performance

Fig. 1a shows photocatalytic inactivation efficiencies of *E. coli* by the Ag/AgX-CNTs photocatalysts with the same dosage under VL irradiation ($\lambda \geq 400$ nm). As a comparison, light control was carried out in the absence of any photocatalysts under VL irradiation, and the bacterial population remained essentially unchanged after 60 min, suggesting that no photolysis occurred for *E. coli*. In the dark controls (with photocatalyst and without light), the density of bacterial remained constant within 60 min, indicating no toxic effect caused to *E. coli* by the photocatalysts alone. When Ag/AgBr-CNTs was irradiated by VL, it exhibited high bactericidal activity and about 1.5×10^7 cfu mL^{-1} of *E. coli* could be completely inactivated within 40 min, which is much faster than those of either Ag/AgCl-CNTs or Ag/AgI-CNTs. The time required for complete inactivation of 1.5×10^7 cfu mL^{-1} of *E. coli* was extent to 50 and 60 min by Ag/AgCl-CNTs and Ag/AgI-CNTs, respectively. The order of photocatalytic disinfection activity is consentience with photocatalytic

degradation of 2, 4, 6-tribromophenol reported in our previous study [30]. In addition, a study reported that Ag^+ at high concentration exhibited bactericidal activity [31]. In this study, however, the Ag^+ was not detected in the reaction solution, meaning that no Ag^+ leakage occurred even after 60 min of photocatalytic reaction for all three photocatalysts. These results suggest that the excellent disinfection activity of Ag/AgX-CNTs should be due to photocatalytic performance of themselves instead of released Ag^+. Similar result of AgBr-Ag-Bi_2WO_6 possessing a high photocatalytc disinfection activity to *E. coli* was also reported by Zhang et al. [24]. The photocatalytic inactivation efficiency of Ag-CNTs with different Ag amount was discussed for the control comparison. As shown in Fig. S3, the density of bacterial remained unchanged after 60 min with 0.0015 and 0.0030 M Ag^+, suggesting that no obvious photocatalytic inactivation occurred in the lower concentration of Ag^+ system. In presence of 0.0150 M Ag^+, about 2-log reductions of cell density were achieved. However, for Ag/AgX-CNTs with 0.0150 M Ag^+ exhibit very excellent photocatalytic inactivation efficiency compared with Ag-CNTs control, indicting synergistic effect of Ag and AgX in this photocatalytic inactivation system.

PL quenching effect is an efficient method to detect the recombination of photogenerated holes and electrons of semiconductor, and was used to analyze the PL property of our synthesized photocatalysts. As shown in Fig. S4, the PL intensity of Ag/AgX-CNTs decreases rapidly compared with that of pure AgX, indicting an significantly decreased the recombination of the photogenerated charges in the photocatalysts because CNTs acted as an excellent electron collector and significantly enhanced the separation efficiency of photogenerated carriers [32]. Overall, introduced CNTs can significantly improve the photogenerated carrier separation efficiency, thus enhance photocatalytic inactivation efficiency.

Generally, photocatalytic inactivation of *E. coli* can be divided into three periods [33,34], the initial period is called the "shoulder", where the reactive species (RSs) begin to attack the *E. coli*, the second period is the main part of photocatalytic process where fast inactivation of bacteria occurs, and the last period is called the "tail", where photocatalytic process is being decelerated. This type of inactivation kinetic process was calculated by the modified Hom model [33].

$$\log\left(\frac{C}{C_0}\right) = -k_1[1-\exp(-k_2 t)]^{k_3}$$

where C and C_0 are the *E. coli* concentration at time; t and t_0, k_1, k_2 and k_3 are kinetic constants at three different period.

This model can be solved using Microsoft Excel tool called GInaFIT [35]. Using this tool, three parameters that represent three steps can be obtained. The S_L (shoulder length) is the incubation time of the first step, k_{max} is the slope of the second step and the n_{res} is the starting point of third deceleration step. Calculating these three parameters can be better to understand the kinetic of inactivation *E. coli*. As shown in Table S1, achieving short incubation period and fast inactivation, without the deceleration period is essential for an efficient photocatalysis process. Notably, the Ag/AgBr-CNTs possesses the lowest inhibition time (S_L) and the fastest inactivation rate (highest k_{max} in the second step) among these three photocatalysts.

To further confirm the VLD photocatalytic disinfection effect of resultant Ag/AgX-CNTs nanocomposites, the BacLight™ kit fluorescent microscopic method was employed [24,36,37], the viable bacterial cells only accumulate SYTO 9, which appears as green fluorescence, while the dead ones with damaged cytoplasmic membranes can accumulate both SYTO 9 and PI, and lead to red fluorescence [24]. The fluorescence assays of untreated and photocatalytically treated *E. coli* were investigated (Fig. 2). In the Ag/AgBr-CNTs-VL system, after being photocatalytically treated for 10 min, some bacterial cells exhibited red fluorescence, indicating their cell membrane was damaged during VLD photocatalytic process. With the prolongation of disinfection reaction, no living bacterial cells were observed after 40 min, and no bacteria revived after 60 min. As expected, photocatalytic bactericidal activities of both Ag/AgCl-CNTs-VL and Ag/AgI-CNTs-VL were much lower, and small partial of the cells were still green within 40 min and almost no living bacteria observed until 60 min treatment (Figs. S5 and S6). Basis on these results, we conclude that Ag/AgX-CNTs nanocomposites possesses excellent VLD photocatalytic disinfection performance.

To better understand the destruction progress of bacteria, the surface structure and morphology of *E. coli* cells at different photocatalytic disinfection stages were also observed using FESEM. As shown in Fig. 3, the untreated *E. coli* exhibited evenly rendered interior of a well-preserved cell wall, while part of central cell wall was obviously damaged when the sample was subjected to 30 min irradiation, indicating initial damage to cell membrane and leading to leakage of interior component such as K^+. These damages occurred mainly can be attributed to the oxidation properties of photocatalytically generated RSs, such as H_2O_2, h^+ and e^- [37]. With further extension of treatment time, much severer damage on the cell structure was observed, the cell wall became greatly ruptured and the intracellular component was severely lost after 120 min. Similar results were also obtained in the Ag/AgCl-CNTs-VL and Ag/AgI-CNTs-VL systems (Figs. S7 and S8). These observations suggest that the destruction process of *E. coli* is beginning from cell envelop.

From above results of live/dead fluorescent and FESEM, it can be confirmed that the cell membrane was severely damaged and intracellular component will be leaked out from the damaged cells during photocatalytic process due to the lack of protection of cell membrane. As known, K^+, an important component existing virtually in bacteria and involving in the regulation of protein synthesis and polysome content, could quickly leak out of bacterial cells during photocatalytic treatment process [24]. The leakage of K^+ is consequently investigated (Fig. 1b). There is almost no significant leakage of K^+ occurred in the dark and light control experiments. In addition, the dark control experiments further confirm our proposal that the inactivation of *E. coli* resulted from the generated h^+, e^- and other RSs during photocatalysis instead of Ag^+. In contrast, in the Ag/AgX-CNTs-VL systems, the amount of K^+ leakage increased in parallel with prolonged inactivation time, and reached a stable value after 40 min. Thus, we can confirm that the cell structure was severely distorted and cell wall was greatly ruptured, subsequently facilitating the entry of large amount of RSs to further decompose the remaining intracellular components. Based on the above evidences, further support the fact that RSs generated in Ag/AgX-CNTs-VL systems could disrupt cell structure, leading to the leakage of intracellular substances and ultimate cell death [24].

To study the effect of wavelengths of VL for these photocatalysts, seven LED lamps with different VL wavelengths were chose. Notably, the light intensity of different wavelengths was kept 10 mW cm^{-2}. As shown in Fig. S9, photocatalytic inactivation efficiencies of *E. coli* were the highest under the irradiation of 435 nm than other wavelengths within the visible-region for all prepared catalysts. Completed inactivation of 7-log bacterial cells was achieved within 60 min irradiation under 435 nm by Ag/AgBr-CNTs. Comparatively, 5- and 4-log bacteria were inactivated by Ag/AgCl-CNTs and Ag/AgI-CNTs, respectively. The 420 nm is the second valid wavelengths next to 435 nm. For instance, 5-, 2- and 2-log reduction of cell density could be achieved within 60 min at 420 nm irradiation when Ag/AgBr-CNTs, Ag/AgCl-CNTs and Ag/AgI-CNTs were used as photocatalysts, respectively. It worth mentioning that under VL with other wavelength irradiation, such as 450, 475, 500, 520 and 550 nm, the reduction of cell density was extremely low, indicating that Ag/AgX-CNTs (X = Cl, Br, I) did

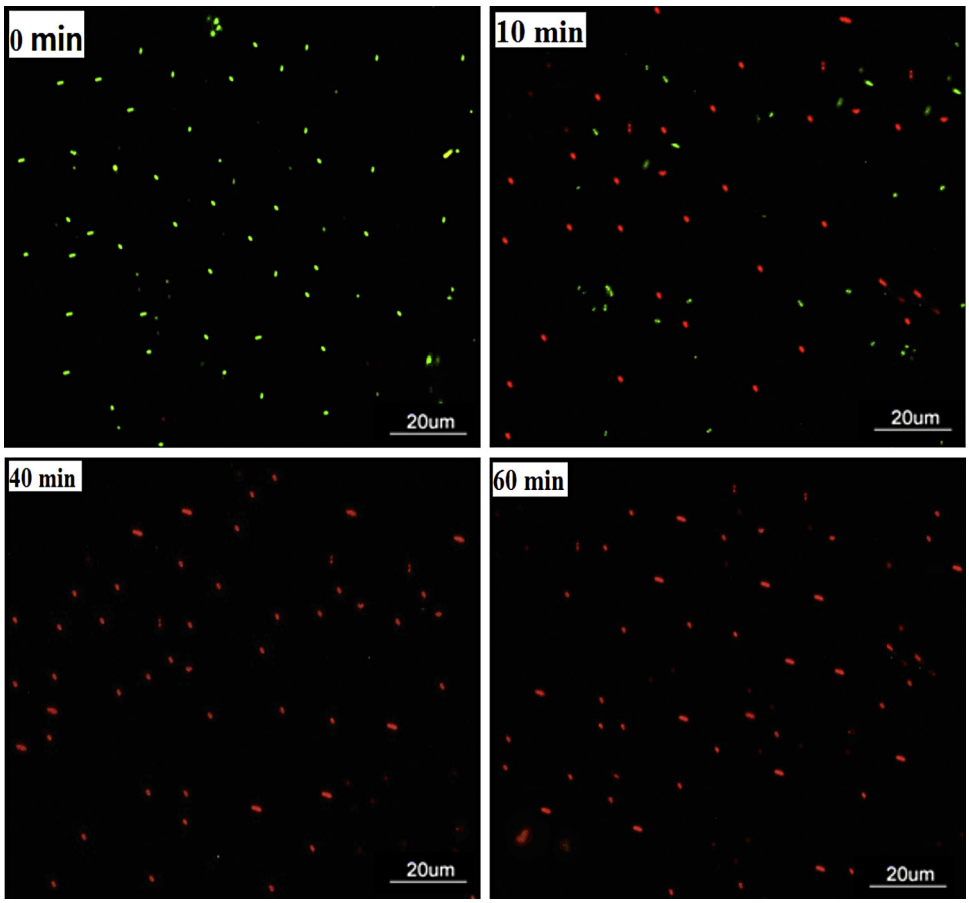

Fig. 2. Fluorescence microscopic images of *E. coli* photocatalytically treated with Ag/AgBr-CNTs under VL irradiation for 0, 10, 40 and 60 min.

not respond to these wavelengths of VL, and subsequently could not inactivate bacteria. To find out the reason as to why photocatalytic inactivation efficiencies under 420 and 435 nm irradiation are much higher than those under different wavelengths, the UV–vis absorption spectra of AgCl, AgBr and AgI were compared (Fig. S10). It can be seen that there is a steep absorption edge at about 445 nm and the absorption intensity of AgBr is stronger than that of AgCl and AgI between the 400 to 445 nm. Therefore, photocatalytic inactivation efficiency of Ag/AgBr-CNTs is higher than those of Ag/AgCl-CNTs and Ag/AgI-CNTs. Also, there was no VL absorption above 450 nm, thus, no reduction of cell density can be expected when the photocatalysts were irradiated by these VL. Although the absorption intensity of the AgX (X = Cl, Br, AgI) under 420 nm is stronger than that of 435 nm, much lower photocatalytic inactivation efficiencies obtained under 420 nm irradiation than those under 435 nm. The probably reason is that the prepared Ag/AgX-CNTs photocatalysts possessed the plasmon absorption band of Ag nanoparticles at about 435 nm during the photocatalytic inactivation process [38,39]. When the photocatalysts were irradiated by VL, Ag nanoparticles were formed in the surface of AgX due to their photosensitivity, and then Ag nanoparticles were also excited by VL because of the localized SPR and generating instant electron–hole pairs on Ag nanoparticles surface, which is benefit to improve photocatalytic activity (Fig. S11).

3.2. Photocatalytic bacterial inactivation mechanism

Photocatalysis is well known to produce various RSs, such as H_2O_2, $^{\bullet}O_2^-$, $^{\bullet}OH$, h^+ and e^-, which were potentially involved in photocatalytic bacterial inactivation process. To determine which were the dominant RSs involved in the VLD bacterial inactivation by Ag/AgX-CNTs, different scavengers were used individually or in combination to remove the respective RSs [40,41]. Taking the Ag/AgBr-CNTs as an example, without addition of any scavenger, about 1.5×10^7 cfu mL^{-1} of *E. coli* could be completely inactivated within 40 min under VL irradiation (Fig. 4). When sodium oxalate (h^+ scavenger) was added, the bacterial cell density only decreased 1-log. This means h^+ contributed to 6-log reduction of bacterial cell density indicating that h^+ is the dominant species involved in photocatalytic inactivation in this system. In the presence of individual scavenger, EDTA-Fe (II) for H_2O_2 and Cr (VI) for e^-, the bacterial cell density decreased about 5- and 4-log, respectively, H_2O_2 and e^- respectively contribution to 2- and 3-log inactivation suggesting that they also play moderate role in this photocatalytic inactivation process. In addition, as reported, the addition of Cr (VI) could remove not only e^- but also part of H_2O_2 by combining O_2 with conduction band e^- [42], and therefore the inactivation efficiency in the presence of Cr (VI) was slightly lower than those adding EDTA-Fe (II). Nevertheless, in the presence of isopropanol ($^{\bullet}OH$ scavenger), the inactivation efficiency did not change much as compared with no scavenger system, indicating that $^{\bullet}OH$ played very a minor role in this process. To further validate the contribution of h^+ in photocatalytic process, isopropanol + EDTA-Fe (II) + Cr (VI) were employed in combination to remove the $^{\bullet}OH$, H_2O_2 and e^- simultaneously, leaving h^+ alone in the system. The presence of only h^+ resulted in a 6-log cell density decrease, further confirming that h^+ is the most important RSs for this photocatalytic inactivation process.

It is of significance for the application of SPR photocatalysts to understand photocatalytic mechanisms of such Ag/AgBr-CNTs photocatalyst. To understand the band structure of AgBr phase, the conduction band (CB) and valence band (VB) energies of AgBr are

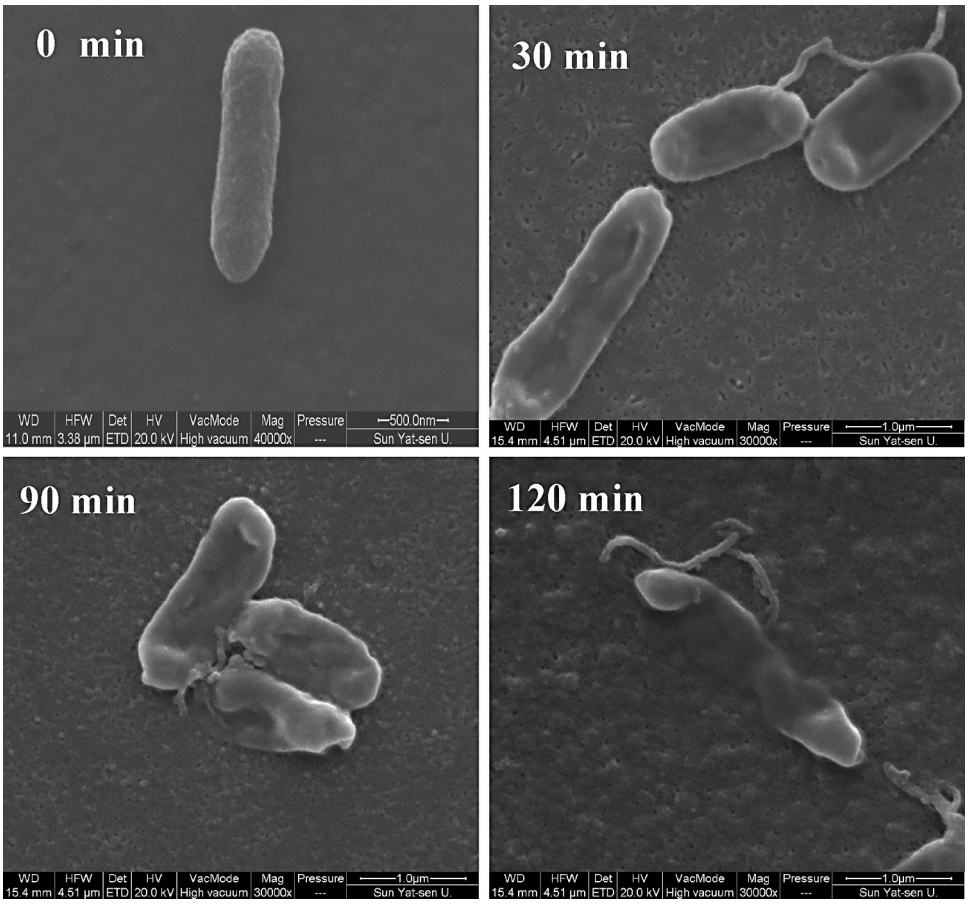

Fig. 3. FESEM images of *E. coli* untreated and photocatalytically treated with Ag/AgBr-CNTs under VL irradiation in different time.

calculated to be about −0.065 and +2.625 V (*vs* SHE), respectively [30]. Therefore, it is possible that the plasmon-induced electrons at Ag nanoparticles of Ag/AgBr-CNTs with a strong reduction power can readily transfer to CB (−0.065 V *vs* SHE) of AgBr [30]. The photocatalytic reaction is initiated by the absorption of VL photons, leading to the generation of electron–hole pairs derived from both photo-excited AgBr and plasmon-excited Ag nanoparticles (Eqs. (1) and (2)). Then charge carriers emigrate to the surface of CNTs under the action of electric field, meanwhile the photogenerated e^- from the plasmon-excited Ag nanoparticles would prefer to flow down to the surface of CNTs crossing the interface due to the dipolar character of the SPR [22]. This promotes the effective separation of photogeneration electron–holes pairs, which can subsequently benefit to improve photocatalytic disinfection activity of the photocatalyst. Therefore, a relative high concentration electrons on the surface of CNTs is formed, which can be trapped by O_2 and H_2O to from H_2O_2 (Eqs. (3)–(5)) [37,43,44]. These RSs, such as h^+, e^- and H_2O_2, could attack the *E. coli*, disrupt cell membrane and result in ultimate cell death (Eq. (6)).

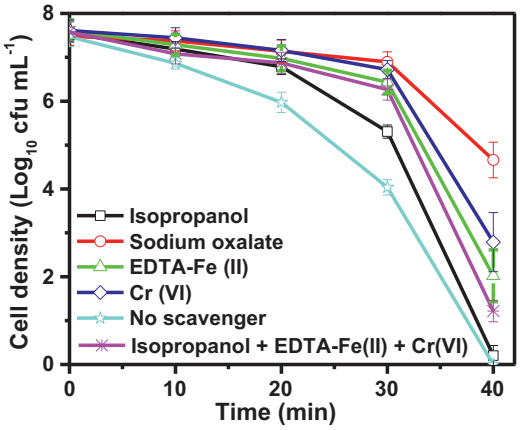

Fig. 4. Photocatalytic inactivation efficiency of *E. coli* by the Ag/AgBr-CNTs with different scavengers (0.1 M Isopropanol, 0.1 M Sodium oxalate, 50 μM Cr (VI), 0.1 mM EDTA-Fe (II)).

$$AgBr + h\nu \rightarrow e^- + h^+ \quad (1)$$

$$Ag + h\nu \rightarrow Ag* \quad (2)$$

$$O_2 + e^- \rightarrow {}^{\bullet}O^{2-} \quad (3)$$

$${}^{\bullet}O^{2-} + H_2O \rightarrow {}^{\bullet}OOH + OH^- \quad (4)$$

$$2{}^{\bullet}OOH \rightarrow O_2 + H_2O_2 \quad (5)$$

$$h^+,\ e^- + H_2O_2 + E.\,coli \rightarrow \text{Organic debris of bacterial cells} \quad (6)$$

Taken together, a plasmon-induced charge-transfer process is presented to improve photocatalytic disinfection activity. As shown in Scheme 1, under VL irradiation, electron–hole pairs are generated on the surface of AgBr, meanwhile, in addition, the electron oscillation occur on the Ag nanocomposite surface owing to SPR, and these e^- transfer from the photoexcited Ag nanoparticles to CB of AgBr, then two part of e^- on CB of AgBr would prefer to flow down to the CNTs crossing the interface. Hence, the lifetime of the charge carriers could be prolonged and the unfavorable recombination of the electron–hole pairs can be successfully hindered. Moreover, the Ag nanoparticles can act as electron traps to suppress electron–hole pair recombination and promote the interfacial charge transfer.

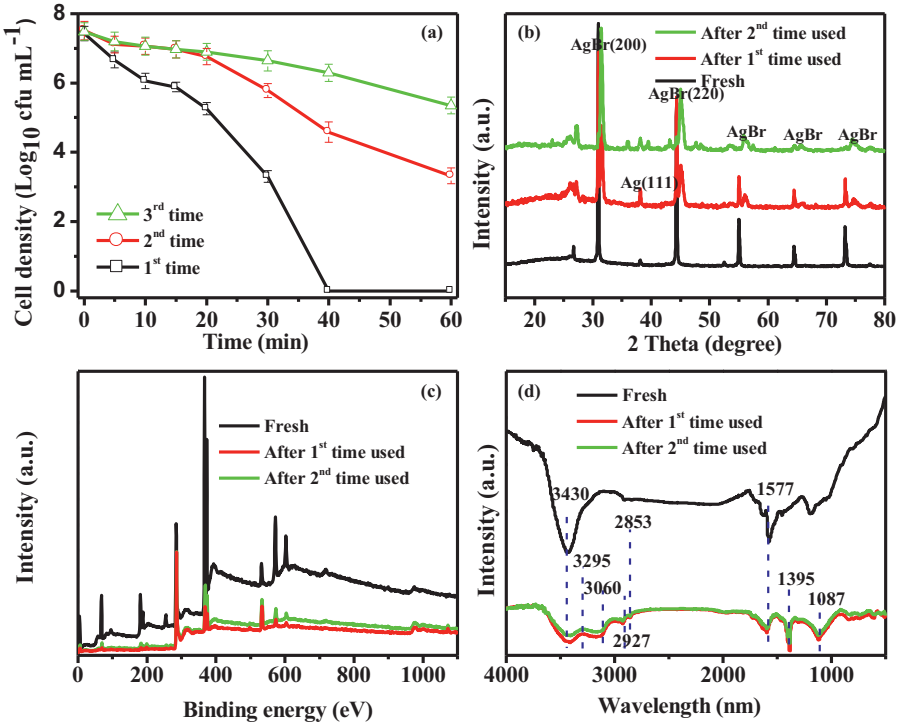

Fig. 5. Cycling photocatalytic inactivation efficiency of *E. coli* over Ag/AgBr-CNTs under VL irradiation (a); XRD (b), XPS (c) and FT-IR (d) spectra of Ag/AgBr-CNTs before and after reuse.

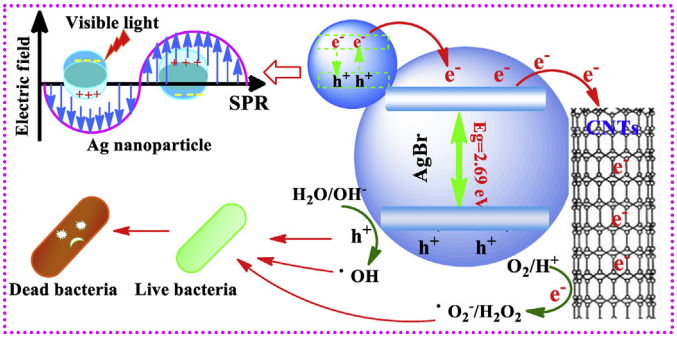

Scheme 1. Schematic photocatalytic inactivation processes and charge transfer of the Ag/AgBr-CNTs photocatalyst under visible light irradiation.

Therefore, more electrons and holes will have opportunity to participate in the disinfection reaction and the inactivation efficiency was enhanced subsequently. The band gap of AgCl and AgI is 2.92 and 2.86 eV, respectively, which is also similar to that of AgBr. So the photocatalytic mechanism of Ag/AgCl-CNTs and Ag/AgI-CNTs should be similar to Ag/AgBr-CNTs.

3.3. Deactivation mechanism of photocatalysts during bacterial inactivation

The stability of the Ag/AgX-CNTs photocatalysts was also investigated by repeating photocatalytic inactivation of *E. coli* experiments with recycled Ag/AgX-CNTs. The recycled Ag/AgX-CNTs photocatalysts were washed twice with distilled water after first photocatalytic treatment before another run. About 1.5×10^7 cfu mL^{-1} of *E. coli* could be completely inactivated within 40 min under the VL irradiation using Ag/AgBr-CNTs as photocatalyst (Fig. 5a). However, the bactericidal activity of Ag/AgBr-CNTs reduced greatly in subsequent usage. For instance, the bacterial cell density only decreased 4- and 2-log when the photocatalyst used in the second and third run, respectively. As for the Ag/AgCl-CNTs and Ag/AgI-CNTs (Fig. S12), their photocatalytic inactivation activities also decreased dramatically in the recycling experiments. Based on these results, it can be concluded that the prepared Ag/AgX-CNTs photocatalysts exhibit significant loss of the inactivation activity after three cycles of repeated experiments. Comparatively, the deactivation of these prepared photocatalysts was much less when they were subjected to organic pollutant degradation [30]. Therefore, it is very necessary to investigate the deactivation mechanism of the photocatalysts to extend theirs lifetime.

The deactivation mechanism of the photocatalysts was studied by characterization of surface properties of the photocatalysts before and after used for photocatalytic bacterial inactivation. According to XRD analysis (Fig. 5b), the Ag/AgBr-CNTs is mainly composed of AgBr (JPCDS file, 06-0438) as well as a spot of metallic Ag (JCPDS file, 65-8428), and the intensity of these peaks is no obviously changed before and after used. Similar results are also obtained for Ag/AgCl-CNTs (Fig. S13), besides the characteristic diffraction peak of Ag (JCPDS file, 65-8428) facets at 37.8°, AgCl phase (JCPDs file, 31-1238) (27.8°, 32.3° and 46.3°) is also observed from XRD patterns of Ag/AgCl-CNTs before and after used twice. As for Ag/AgI-CNTs (Fig. S13), the peaks in XRD patterns are also characterized as AgI (JCPDS file, 09-0388). In addition, the surface properties of the photocatalysts before and after used were also characterized by XPS (Figs. 5c, S14 and S15). There was no change of Ag/AgX-CNTs before and after used, which is agreed with the result of XRD analysis. Based on above results, it can be confirmed that the main phase structure and surface properties of the photocatalysts do not show obviously difference for the photocatalysts before and after photocatalytic inactivation. This result is slightly different from the result of our previous study in organics degradation, which showed that the diffraction intensity of AgBr decreased slightly with the increase of the reusing times of photocatalyst. In contrast, the diffraction intensity of Ag(0) increases slightly [30].

Theoretically, if there was no obvious change of the surface properties of the photocatalysts before and after used for *E. coli* inactivation, it should not lead to so sharp decrease of photocatalytic disinfection activity during the multi-run recycling experiments. Therefore, more in-depth study on the surface elemental composition of the photocatalysts before and after treatment of *E. coli* was conducted by FT-IR analysis (Figs. 5d and S16). There are some different absorption peaks on the surface of photocatalysts before and after use. On the Ag/AgX-CNTs (X = Cl, Br, I) surface after treating *E. coli*, two peaks at ~3295 and 3060 cm^{-1} were assigned to amide A and amide B, respectively [45]. While the peaks at 2927 and 2853 cm^{-1} were assigned to υ_a (CH_2) and υ_s (CH_2), respectively. A wide peak at about 3430 cm^{-1} due to the OH^- vibration of the absorbed water. The peak of 1096 cm^{-1} also well matched the assignment for the vibration of the sugar rings of the lipopolysaccharide [20,45]. The bands at around 1395 cm^{-1} was assigned to the $-COO^-$ group of the fatty acid, as well as the band near the 1577 cm^{-1} due to the glutamate carboxylate stretching, the band around the 1087 cm^{-1} attribute to oligosaccharide [45]. From above all data analyzed, it can be implied that *E. coli* cells were not only killed but also destructed to large biomolecules in photocatalytic system. These results are well agreed with our previous characterizations, like FESEM and K^+ leakage. Thus, it can be conclude that, during photocatalytic inactivation of bacteria, the cell structure was severely distorted and greatly ruptured, and the organic debris of the decomposed bacterial cells might be adsorbed onto the surface of photocatalysts, which might block the active sites of photocatalysts leading to the decrease photocatalytic activity. Therefore, the deactivation mechanism of Ag/AgX-CNTs might different during photocatalytic inactivation of bacteria and degradation of organics as presented in our previous study [30]. Previous results showed that the slight reduce of photocatalytic performance during the photocatalyst recycling reactions might be the loss of small part of Ag^+ on the photocatalyst surface during light irradiation, since Ag^+ could be reduced to metallic Ag(0) by photogenerated e^-. Unlike large biomolecule, small organic molecule like tribromophenol could not block the active sites of photocatalysts. Furthermore, most of the tribromophenol degradation intermediates of are hydrophilic and readily dissolve in the reaction solution rather than adsorption on the photocatalyst surface.

4. Conclusion

In summary, we highlight an available pathway to photocatalytic disinfection under VL irradiation by using a series of systhesized Ag/AgX-CNTs (X = Cl, Br, I) composites. A excellent photocatalytic disinfection performance of Ag/AgX-CNTs was achieved due to the localized SPR of Ag nanoparticles and the efficient photogeneraed carrier separation owing to the CNTs introduced. In addition, the results of stability and deactivation mechanism of Ag/AgX-CNTs showed that the organic debris of decomposed bacteria may be blocked the active sites of the photocatalysts leading to the decrease of the photocatalytic activity. The application of the Ag/AgX-CNTs photocatalytic disinfection will facilitate development of reliable disinfection technology.

Acknowledgments

This is contribution no. IS–1873 from GIGCAS. This work was supported by NSFC (41373103 and 21077104), NSFC-Guangdong Joint Funds (U1201234), China Postdoctoral Science Foundation (2012M511843), and a research grant (GRF476811) of Research Grant Council, Hong Kong SAR Government to P.K. Wong.

Appendix A. Supplementary data

Supplementary data associated with this article can be found, in the online version, at http://dx.doi.org/10.1016/j.apcatb.2014.04.033.

References

[1] L. Ye, J. Liu, C. Gong, L. Tian, T. Peng, L. Zan, ACS Catal. 2 (2012) 1677–1683.
[2] L.S. Zhang, K.H. Wong, D.Q. Zhang, C. Hu, J.C. Yu, C.Y. Chan, P.K. Wong, Environ. Sci. Technol. 43 (2009) 7883–7888.
[3] W.J. Wang, L.Z. Zhang, T.C. An, G.Y. Li, H.Y. Yip, P.K. Wong, Appl. Catal. B: Environ. 108–109 (2011) 108–116.
[4] M.G. Muellner, E.D. Wagner, K. McCalla, S.D. Richardson, Y.-T. Woo, M.J. Plewa, Environ. Sci. Technol. 41 (2006) 645–651.
[5] M.A. Radzig, V.A. Nadtochenko, O.A. Koksharova, J. Kiwi, V.A. Lipasova, I.A. Khmel, Colloid Surf. B: Biointerfaces 102 (2013) 300–306.
[6] T. Matsunaga, R. Tomoda, T. Nakajima, H. Wake, FEMS Microbiol. Lett. 29 (1985) 211–214.
[7] D.S. Kim, S.Y. Kwak, Environ. Sci. Technol. 43 (2008) 148–151.
[8] J.C. Yu, W. Ho, J. Yu, H. Yip, P.K. Wong, J. Zhao, Environ. Sci. Technol. 39 (2005) 1175–1179.
[9] Q. Li, R. Xie, Y.W. Li, E.A. Mintz, J.K. Shang, Environ. Sci. Technol. 41 (2007) 5050–5056.
[10] F. Chen, X. Yang, Q. Wu, Environ. Sci. Technol. 43 (2009) 4606–4611.
[11] Z. Zhang, W. Wang, E. Gao, S. Sun, L. Zhang, J. Phys. Chem. C 116 (2012) 25898–25903.
[12] X. Hu, C. Hu, T. Peng, X. Zhou, J. Qu, Environ. Sci. Technol. 44 (2010) 7058–7062.
[13] D. Tsukamoto, Y. Shiraishi, Y. Sugano, S. Ichikawa, S. Tanaka, T. Hirai, J. Am. Chem. Soc. 134 (2012) 6309–6315.
[14] M.S. Zhu, P.L. Chen, M.H. Liu, ACS Nano 5 (2011) 4529–4536.
[15] R.H. Li, W.X. Chen, H. Kobayashi, C.X. Ma, Green Chem. 12 (2010) 212–215.
[16] Y. Tian, T. Tatsuma, J. Am. Chem. Soc. 127 (2005) 7632–7637.
[17] M.S. Zhu, P.L. Chen, M.H. Liu, Langmuir 28 (2012) 3385–3390.
[18] Y. Hou, F. Zuo, Q. Ma, C. Wang, L. Bartels, P. Feng, J. Phys. Chem. C 116 (2012) 20132–20139.
[19] C. Hu, Y. Lan, J. Qu, X. Hu, A. Wang, J. Phys. Chem. B 110 (2006) 4066–4072.
[20] Y. Hou, X. Li, Q. Zhao, G. Chen, C.L. Raston, Environ. Sci. Technol. 46 (2012) 4042–4050.
[21] S. Linic, P. Christopher, D.B. Ingram, Nat. Mater. 10 (2011) 911–921.
[22] Y.H. Zhang, Z.R. Tang, X.Z. Fu, Y.J. Xu, Appl. Catal. B 106 (2011) 445–452.
[23] H.X. Shi, T.Y. Zhang, H.L. Wang, X. Wang, M. He, Chin. J. Catal. 32 (2011) 46–50.
[24] L.S. Zhang, K.H. Wong, H.Y. Yip, C. Hu, J.C. Yu, C.Y. Chan, P.K. Wong, Environ. Sci. Technol. 44 (2010) 1392–1398.
[25] T.C. An, J.Y. Chen, X. Nie, G.Y. Li, H.M. Zhang, X.L. Liu, H.J. Zhao, ACS Appl. Mater. Interfaces 4 (2012) 5988–5996.
[26] N. Bouazza, M. Ouzzine, M.A. Lillo-Ródenas, D. Eder, A. Linares-Solano, Appl. Catal. B: Environ. 92 (2009) 377–383.
[27] D. Xu, P. Lu, P. Dai, H. Wang, S. Ji, J. Phys. Chem. C 116 (2012) 3405–3413.
[28] J.Y. Chen, G.Y. Li, Y. Huang, H.M. Zhang, H.J. Zhao, T.C. An, Appl. Catal. B: Environ. 123–124 (2012) 69–77.
[29] B. Liu, H.C. Zeng, Chem. Mater. 20 (2008) 2711–2718.
[30] H.X. Shi, J.Y. Chen, G.Y. Li, X. Nie, H.J. Zhao, P.K. Wong, T.C. An, ACS Appl. Mater. Interfaces 5 (2013) 6959–6967.
[31] Y.K.T. Sukdeb Pal, Joon Myong Song, Appl. Environ. Microbiol. 73 (2007) 1712–1720.
[32] B. Pan, D. Cui, C.S. Ozkan, M. Ozkan, P. Xu, T. Huang, F. Liu, H. Chen, Q. Li, R. He, F. Gao, J. Phys. Chem. C 112 (2008) 939–944.
[33] N. Baram, D. Starosvetsky, J. Starosvetsy, M. Epshtein, Electrochim. Acta 54 (2009) 3381–3386.
[34] N. Baram, D. Starosvetsky, J. Starosvetsky, M. Epshtein, R. Armon, Y. Ein-Eli, Appl. Catal. B: Environ. 101 (2011) 212–219.
[35] J. Marugán, R. van Grieken, C. Sordo, C. Cruz, Appl. Catal. B: Environ. 82 (2008) 27–36.
[36] R. Van Grieken, J. Marugán, C. Pablos, L. Furones, A. López, Appl. Catal. B: Environ. 100 (2010) 212–220.
[37] H.X. Shi, T.Y. Zhang, B. Li, X. Wang, M. He, M.Y. Qiu, Catal. Commun. 12 (2011) 1022–1026.
[38] T. Hirakawa, P.V. Kamat, Langmuir 20 (2004) 5645–5647.
[39] M.R. Jones, K.D. Osberg, R.J. Macfarlane, M.R. Langille, C.A. Mirkin, Chem. Rev. 111 (2011) 3736–3827.
[40] H.S. Fang, Y.P. Gao, G.Y. Li, J.B. An, P.K. Wong, H.Y. Fu, S.D. Yao, X.P. Nie, T.C. An, Environ. Sci. Technol. 47 (2013) 2704–2712.
[41] W.J. Wang, T.W. Ng, W.K. Ho, J.H. Huang, S.J. Liang, T.C. An, G.Y. Li, J.C. Yu, P.K. Wong, Appl. Catal. B: Environ. 129 (2013) 482–490.
[42] Y.M. Chen, A.H. Lu, Y. Li, L.S. Zhang, H.Y. Yip, H.J. Zhao, T.C. An, P.K. Wong, Environ. Sci. Technol. 45 (2011) 5689–5695.
[43] Q. Zhu, W.S. Wang, L. Lin, G.Q. Gao, H.L. Guo, H. Du, A.W. Xu, J. Phys. Chem. C 117 (2013) 5894–5900.
[44] P. Wang, B. Huang, X. Qin, X. Zhang, Y. Dai, J. Wei, M.-H. Whangbo, Angew. Chem. Int. Ed. 47 (2008) 7931–7933.
[45] J. Kiwi, V. Nadtochenko, Langmuir 21 (2005) 4631–4641.